Available online at www.sciencedirect.com
ScienceDirect
Journal of Power Sources 161 (2006) 1041–1055
JOURNAL OF POWER SOURCES
www.elsevier.com/locate/jpowsour

# Optimization of a PEM fuel cell system based on empirical data and a generalized electrochemical semi-empirical model

J. Wishart, Z. Dong *, M. Secanell

*Department of Mechanical Engineering and Institute for Integrated Energy Systems, University of Victoria, Victoria, BC, Canada V8W 3P6*

Received 10 March 2006; received in revised form 16 May 2006; accepted 16 May 2006
Available online 17 August 2006

**Abstract**

A systematic method to obtain the optimal operating conditions of a fuel cell system is presented. This method is based on the coupling of a semi-empirical fuel cell stack model and an associated balance of plant (BOP) model with an optimization algorithm in order to efficiently explore the range of possible operating conditions. The approach described in the paper to obtain optimal operating conditions is applied to a fuel cell system designed to operate in two different applications: automotive and stationary. In both cases, the application of this methodology results in a set of optimal operating conditions that yields large improvements in the system performance. The optimization problem is solved for two different performance objectives: maximization of net system power and maximization of system exergetic efficiency.


*Keywords:* PEM fuel cell; Optimization; Fuel cell modeling; System modeling

## 1. Introduction

As a promising technology that may successfully supersede the combustion of fossil fuels as the dominant method of energy conversion, hydrogen fuel cells are studied worldwide with an aim to improve the power output, lower the cost and extend the life of operation for widespread applications.

Among various types of fuel cells, the proton exchange membrane fuel cell (PEMFC) is arguably the fastest-growing type and the fuel cell that is most likely to be widely used in the near future. The modeling and optimization of a PEMFC system, carried out in this work, is aimed at achieving better performance of a given fuel cell system design.

### 1.1. Stack modeling

Modeling of real-world applications has been seen as a useful tool for decades. Fuel cell and fuel cell system modeling is in its relative infancy, but already a significant amount of effort has been put forth to understand the parameters and issues affecting the performance of the fuel cell system.

There are several types of modeling approaches, and the line separating these approaches is often blurry. Essentially however, the approaches may be classified as: (a) theoretical, sometimes known as 'mechanistic'; (b) computational fuel cell dynamics (CFCD) simulation; (c) semi-empirical; (d) empirical depending on the level of modeling sophistication. Each approach has advantages and disadvantages, as discussed in [1].

In this work, since the main interest is in the development of a methodology to obtain the optimal fuel cell system operating conditions and not on the fuel cell design itself, a simple but computationally inexpensive model is used. In particular, the semi-empirical approach based on work by researchers at the Royal Military College (RMC) is chosen [2–5]. The RMC model is robust and flexible and is primarily steady-state but also has simplified transient aspects. The RMC model has been used by members of industry, where Ballard Power Systems is the most notable example [6], and by other research groups [7] that have incorporated early versions of the model and used experimentation to validate its veracity. The model has achieved an accuracy and adaptability that has allowed it to be deemed functional for the current research.

In order to make this semi-empirical model as accurate as possible, over the past 10 years, considerable work has been done to acquire the empirical model parameters of the benchmark Ballard MK4 and MK5 stacks. Extensive tests have also been

* Corresponding author. Tel.: +1 250 721 8900; fax: +1 250 721 6051.
*E-mail address:* zdong@me.uvic.ca (Z. Dong).

0378-7753/$ – see front matter © 2006 Elsevier B.V. All rights reserved.
doi:10.1016/j.jpowsour.2006.05.056

## Nomenclature

$A_{active}$ active cell area ($cm^2$)
$A_{cell}$ radiative stack area ($cm^2$)
$A_{Ends}$ area of fuel cell stack ends ($cm^2$)
$A_{Sides}$ area of fuel cell stack sides ($cm^2$)
$A_t$ total stack cross-sectional area ($cm^2$)
$c_{p_{air}}$ specific heat of air at constant pressure ($J\,K^{-1}\,kg^{-1}$)
$c_{p_{H_2O}}$ specific heat of water at constant pressure ($4128\,J\,K^{-1}\,kg^{-1}$)
$C_{O_2}^{Interface}$ concentration of oxygen gas at the surface of the catalyst at the cathode
ex exergy ($kJ\,mol^{-1}$)
$ex_{CH}$ chemical exergy ($kJ\,mol^{-1}$)
$ex_{KE}$ kinetic energy exergy ($kJ\,mol^{-1}$)
$ex_{PE}$ potential energy exergy ($kJ\,mol^{-1}$)
$E_{max}$ maximum voltage obtained from converting enthalpy of formation of hydrogen into electrical energy (1.48 V)
$E_{Nernst}$ Nernst voltage (V)
$f(\mathbf{x}, i)$ objective function
$F$ Faraday constant ($96{,}485\,C\,electron^{-1}$)
$h$ specific enthalpy ($kJ\,mol^{-1}$)
$h_{conv}$ heat transfer coefficient of convection ($W\,m^{-2}\,K^{-4}$)
$h_{conv,bottom}$ heat transfer coefficient of convection of fuel cell channel bottom ($W\,m^{-2}\,K^{-4}$)
$h_{conv,top}$ heat transfer coefficient of convection of fuel cell channel top ($W\,m^{-2}\,K^{-4}$)
$h_{prod,j}$ enthalpy of product $j$ ($kJ\,mol^{-1}$)
$h_{react,i}$ enthalpy of reactant $i$ ($kJ\,mol^{-1}$)
$h_0$ enthalpy of reference environmental (restricted) state ($kJ\,mol^{-1}$)
$i$ fuel cell current density ($A\,cm^{-2}$)
$I$ fuel cell current (A)
$I_L$ current at which hydrogen consumption is equal to hydrogen supply (A)
$l_{vap}$ latent heat of vaporization ($J\,kg^{-1}$)
$\dot{m}_{air}$ mass flow of air ($kg\,s^{-1}$)
$\dot{m}_{cool,H_2O}$ mass flow of water required for cooling ($kg\,s^{-1}$)
$\dot{m}_{H_2}$ mass flow of hydrogen gas ($kg\,s^{-1}$)
$\dot{m}_{H_2O,heat\ exchanger}$ mass flow of water in heat exchanger ($kg\,s^{-1}$)
$\dot{m}_{H_2O,in\ air}$ mass flow of water required for air stream humidification ($kg\,s^{-1}$)
$\dot{m}_{H_2O,in\ H_2}$ mass flow of water required for hydrogen stream humidification ($kg\,s^{-1}$)
$\dot{m}_{H_2O,produced}$ rate of water produced at cathode ($kg\,s^{-1}$)
$M_{air}$ molar mass of air ($28.97 \times 10^{-3}\,kg\,mol^{-1}$)
$M_{H_2}$ molar mass of hydrogen ($2.016 \times 10^{-3}\,kg\,mol^{-1}$)
$M_{H_2O}$ molar mass of water ($18.018 \times 10^{-3}\,kg\,mol^{-1}$)
$n_{cell}$ number of fuel cells in the stack
$\dot{N}_{H_2}$ molar flow of hydrogen gas at inlet ($mol\,s^{-1}$)
$\dot{N}_{H_2,out}$ molar flow of hydrogen gas at outlet ($mol\,s^{-1}$)
$\dot{N}_{O_2}$ molar flow of oxygen gas at inlet ($mol\,s^{-1}$)
$\dot{N}_{prod,j}$ molar flow of product $j$ ($mol\,s^{-1}$)
$\dot{N}_{react,i}$ molar flow of reactant $i$ ($mol\,s^{-1}$)
$p_{H_2}^{interface}$ pressure of hydrogen gas at surface of the catalyst at the anode (bar)
$p_{O_2}^{interface}$ pressure of oxygen gas at surface of the catalyst at the cathode (bar)
$p_{H_2O}^{sat}$ saturation pressure of water vapour at a given temperature (bar)
$P_{air,atm}$ atmospheric pressure (101.325 kPa)
$P_{cell}$ fuel cell operating pressure (bar)
$P_{drop,coolant}$ pressure drop of coolant through cooling loop (bar)
$P_{drop,humid}$ pressure drop of water through humidification stream (bar)
$r_M$ membrane-specific resistivity for the flow of hydrated protons ($\Omega\,cm$)
$R$ universal gas constant ($8.3145\,J\,mol^{-1}\,K^{-1}$)
$R^{electronic}$ ohmic electronic overvoltage resistance ($\Omega\,cm^2$)
$R^{protonic}$ ohmic protonic overvoltage resistance ($\Omega\,cm^2$)
$\dot{Q}_{air,total}$ heat lost to air stream and surroundings (W)
$\dot{Q}_{conv,total}$ heat lost to air stream due to convection (W)
$\dot{Q}_{conv,top+bottom}$ heat lost to convection at the fuel cell channel top and bottom (W)
$\dot{Q}_{conv,walls}$ heat lost to convection at the fuel cell channel walls (W)
$\dot{Q}_{evap}$ heat lost to air stream due to evaporation (W)
$\dot{Q}_{rad}$ heat lost to surroundings due to radiation (W)
$\dot{Q}_{total}$ heat produced due to electrochemical reaction (W)
$s$ specific entropy ($kJ\,mol^{-1}\,K^{-1}$)
$s_0$ entropy of reference environmental (restricted) state ($kJ\,mol^{-1}\,K^{-1}$)
$t$ thickness of membrane (cm)
$T_{cell}$ fuel cell operating temperature (K)
$T_{cool,H_2O,in}$ temperature of coolant water at inlet (K)
$T_0$ ambient air temperature (K)
$V_{cell}$ output voltage of single fuel cell (V)
$W_{compressor}$ power consumed by the compressor (W)
$W_{cool,pump}$ power consumed by the coolant pump (W)
$W_{humid,pump}$ power consumed by the humidifier pump (W)
$W_{gross,stack}$ gross power output of fuel cell stack (W)
$w_j$ weighting of objective $j$
$W_i(\mathbf{x}, i)$ net power at current density $i_j$ for objective $j$ (W)
$W_{net,parasitic}$ net parasitic power lost (W)
$W_{net,system}$ net power output of fuel cell system (W)
$\mathbf{x}$ design variable vector
$x_j$ molar fraction of substance $j$
$\mathbf{x}_{max}$ upper limit vector of design variable
$\mathbf{x}_{min}$ lower limit vector of design variable
$x_{H_2O}^{sat}$ molar fraction of water in a gas stream for a given temperature
$x_{other\ gases}^{channel}$ molar fraction of gases (apart from oxygen) in the air stream

$x^{\text{in,hum}}_{\text{othergases}}$ molar fraction of gases (apart from oxygen) at the inlet
$x^{\text{out,hum}}_{\text{other gases}}$ molar fraction of gases (apart from oxygen) at the outlet

*Greek symbols*

$\beta_1$ empirical term in activation overvoltage equation (V)
$\beta_2$ empirical term in activation overvoltage equation ($\text{V K}^{-1}$)
$\beta_3$ empirical term in activation overvoltage equation ($\text{V K}^{-1}$)
$\beta_4$ empirical term in activation overvoltage equation ($\text{V K}^{-1}$)
$\gamma$ isentropic compression ratio
$\Delta H$ change in enthalpy (kJ)
$\eta_{\text{act}}$ activation overvoltage (V)
$\eta_{\text{conc}}$ concentration overvoltage (V)
$\eta_{\text{motor}}$ efficiency of model pump motors
$\eta_{\text{ohmic}}$ ohmic overvoltage (V)
$\eta_{\text{pump}}$ efficiency of model pumps
$\eta_{\text{system,energy}}$ system energy (1st law) efficiency
$\eta_{\text{system,exergetic}}$ system exergetic (2nd law) efficiency
$\eta^{\text{electronic}}_{\text{ohmic}}$ ohmic electronic overvoltage
$\eta^{\text{protonic}}_{\text{ohmic}}$ ohmic protonic overvoltage
$\lambda_{\text{air}}$ air stoichiometry (≡ oxygen stoichiometry)
$\lambda_{H_2}$ hydrogen stoichiometry
$\lambda_{\text{membrane}}$ empirical parameter that describes membrane conditions
$\lambda_{O_2}$ oxygen stoichiometry (≡ air stoichiometry)
$\mu_{j0}$ chemical potential of substance $j$ at reference environmental (restricted) state ($\text{kJ mol}^{-1}$)
$\mu_{j00}$ chemical potential of substance $j$ at reference dead environmental (unrestricted) state ($\text{kJ mol}^{-1}$)
$\rho_{H_2O}$ density of water ($998\ \text{kg m}^3$)

carried out in the author's group to acquire the model parameters for the new close-to-ambient pressure PEM fuel stack designs, including the tri-flow, external-manifold, radiator stack (TERS), developed by the group [8–10], and the PC6-1200 stack from Palcan Power Systems [11,12].

A PC6-1200 stack has been installed as part of a power system in a low-speed fuel cell hybrid electric vehicle (LSFCHEV). This LSFCHEV will undergo performance testing using a dynamometer platform that will provide indirect system data, and the system itself will be tested separately to complement the data set and measure the accuracy of the system model. Subsequent publications will include discussion and results from these tests. The data obtained from the stack testing of the three aforementioned stacks have been used to determine the model parameters associated with each particular stack, and the results are presented in Section 3.1. The current work is the first step in developing a virtual prototype of the LSFCHEV that will undergo extensive simulation and sensitivity analysis before the physical prototype is tested to validate the simulation results.

### 1.2. System optimization

Given the complexity of fuel cell modeling, fuel cell and fuel cell system optimization presents a real technical challenge. Nevertheless, some laudable attempts at fuel cell optimization can be found in the literature. Grujicic and Chittajallu [13] used a two-dimensional computational fuel cell dynamics model of a single fuel cell to optimize the electric current per fuel cell width at a cell voltage of 0.7 V. In the optimization, sequential quadratic programming was used to obtain the operational and geometric parameters for achieving the maximum electric current, including air inlet pressures and cathode thickness, cathode length for each shoulder segment of flow channel, and fraction of cathode length associated with the flow channel. More recently, Mawardi et al. [14] employed a numerical one-dimensional fuel cell model to optimize the power density with respect to several operating parameters. The optimization allowed for quantitative discussion of the effects of membrane and electrode thicknesses and CO concentration on the values of the optimum operating conditions. At the fuel cell system level, however, the only two attempts at optimization were done by Xue and Dong [6], and Wang et al. [15]. Xue and Dong used a semi-empirical model of the Ballard Mark IV fuel cell and models for the auxiliary systems to create a model of the fuel cell system. Using this model and numerical optimization, the optimal active stack area and air stoichiometric ratio was obtained to maximize net power output, and, at the same time, minimized production costs. Wang and Dong performed an optimization on a fuel cell system as a demonstration of a novel optimization algorithm [8,15]. The optimization results showed an improvement in system efficiency, net power, volumetric and gravimetric power densities, as well as in a reduction of system costs.

In general, optimization of fuel cell systems is still a challenge not only because of the inaccuracy of the models but because the optimization is a highly non-linear problem where the objective function is calculated using a numerical model of the fuel cell and fuel cell system. Non-linear optimization involves the search for a minimum of a non-linear objective function subject to non-linear constraints. It is common for these optimization problems to have multiple optima. At present, two different search approaches have emerged in the area of non-linear design optimization: local methods and global methods.

Local methods aim to obtain a local minimum, and they cannot guarantee that the minimum obtained is the absolute minimum for a non-unimodal objective function and/or a non-convex feasible region. These methods are usually first-order methods. Some of the most popular local methods for optimization include the conjugate gradient algorithms and the quasi-Newton methods for unconstrained optimization and the sequential linear and quadratic programming methods for constrained optimization. Although local methods do not aim for the global optima, several approaches can be used to continue searching once a local minimum has been located to obtain the global optima, such as

the stochastic based approaches of random multi-start methods [16,17] and ant colony searches [18].

Global methods aim to obtain the global minimum of the function. Mostly based on stochastic procedures, these methods do not need any information about the gradient. Some of the most popular methods for global optimization are genetic algorithms (GA), simulated annealing (SA), tabu search, and stochastic programming.

In this work, one local optimization algorithm and two global optimization algorithms are coupled to a fuel cell system model in order to explore the design space and to guarantee a solution that is independent on the method used. The three-optimization techniques are: sequential quadratic programming (SQP), simulated annealing (SA) and genetic algorithms (GA). The optimization algorithms use operating parameters such as the temperature, pressure ratios and the stoichiometries of the reactants as design variables. These optimization routines are used to search for the best operating parameters that lead to peak fuel cell system performance. This work has focused on obtaining the optimal operating conditions of the fuel cell system and not on obtaining optimal physico-chemical parameters of the fuel cell. These are two different goals. The objective of the current work is to show a method to select, for a given fuel cell, the best operating parameters. Optimizing the physico-chemical parameters, while also an extremely useful and necessary endeavour, has the goal of improving the actual design of the fuel cell and stack; future work should combine the optimization of operating and physico-chemical parameters resulting in a truly optimized fuel cell system.

## 2. Fuel cell system model

The PEMFC stack model implemented in this work is based on the work at the Royal Military College of Canada by Amphlett et al. [2,3], Mann et al. [4] and Fowler et al. [5]. The model, known as the generalized steady-state electrochemical model (GSSEM), is zero-dimensional, semi-empirical, isothermal and static in nature; thus, the parameters of the equations are determined experimentally to provide the time-independent polarisation curves, power curves and system efficiencies at various operating conditions. The stack model is integrated into the larger fuel cell system model with its constituent BOP components, and the resultant model is able to calculate the net output power of the system. A schematic representation of the fuel cell system is shown in Fig. 1.

### 2.1. Fuel cell model

The fuel cell model is for a PEMFC, which uses the following electrochemical reaction:

$$H_2 + \frac{1}{2}O_2 \leftrightarrow H_2O \tag{1}$$

where the reaction is exothermic.

The voltage of the fuel cell, $V_{cell}$, is modeled as [4]

$$V_{cell} = E_{Nernst} + \eta_{act} + \eta_{ohmic} + \eta_{conc} \tag{2}$$

where $E_{Nernst}$ is the Nernst equation, which is an expression for the electromotive force (EMF) for given product and reactant activities; $\eta_{act}$ the activation overvoltage, which is the amount of voltage used to drive the reaction; $\eta_{ohmic}$ the ohmic overvoltage, which is the amount of voltage lost to the resistance to electron flow in the electrodes and the resistance to ion flow in the electrolyte; $\eta_{conc}$ is the concentration overvoltage, which is the voltage lost when the concentration of reactant at the electrode is diminished. In Eq. (2), the overpotentials are all positive because they are assumed to be losses of the fuel cell. This is in accordance with the derivation in Ref. [2], where a more detailed

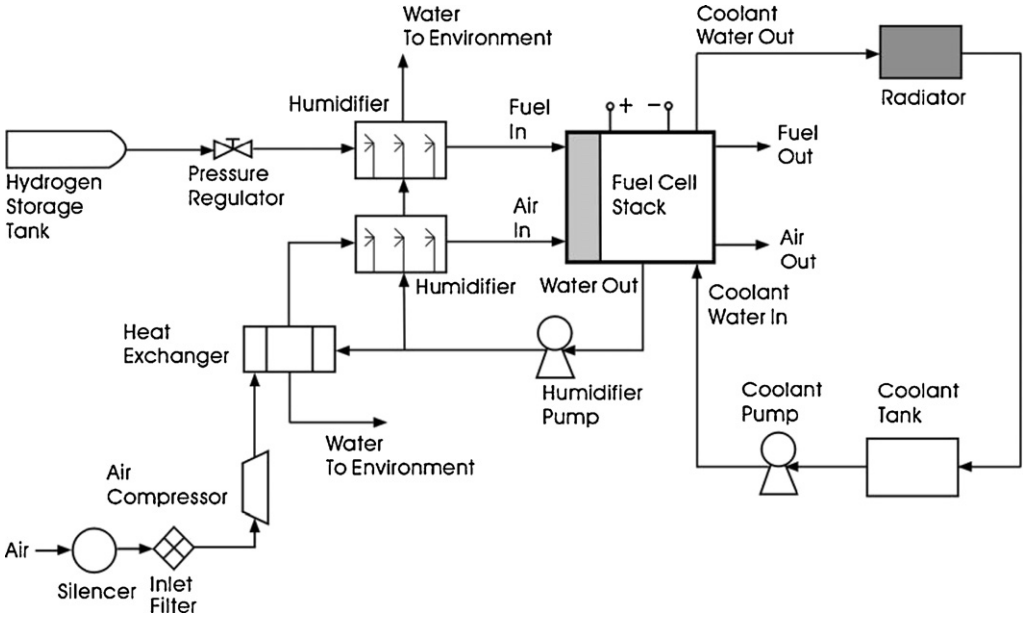


Fig. 1. Fuel cell system schematic layout.

explanation of how these terms are obtained based on electrochemical arguments is given. The terms of Eq. (2) are discussed in the following sections for the sake of completeness.

The output of the fuel cell system will depend strongly on the amount of reactants input into the system; the relative amounts that take part in the electrochemical reaction of Eq. (1) are dictated by the molar balance of this equation. The molar mass flow of $H_2$ is given by

$$\dot{N}_{H_2} = \frac{I\lambda_{H_2} n_{cell}}{2F} \tag{3}$$

where $\lambda_{H_2}$ is the stoichiometry of the hydrogen gas and $F$ is Faraday's constant. The corresponding expression for the molar mass flow of oxygen is

$$\dot{N}_{O_2} = \frac{I\lambda_{O_2} n_{cell}}{4F} \tag{4}$$

The oxygen flow comes from the ambient air brought into the compressor such that $\lambda_{air}$ is equal to $\lambda_{O_2}$.

The production of water is both a benefit and a hindrance to the operation of the fuel cell, as a delicate balance must be struck between having enough moisture to maintain the humidity of the membrane while also ensuring that the MEA is not flooded with excess water. Either situation will result in a reduction in the efficacy of the fuel cell operation. If the membrane dries out, the proton conductivity and oxygen reaction kinetics decrease temporarily, but excessive dehydration can result in permanent damage to the membrane and permanently impaired power production. The model used in this work assumes that the membrane is fully hydrated without any water management issues, an assumption justified in other work [18]. The water produced at the cathode is used to externally humidify the reactants, as shown in Fig. 1, and the equation for water production is given by [19]

$$\dot{m}_{H_2O,produced} = \frac{In_{cell} M_{H_2O}}{2F} \tag{5}$$

where $M_{H_2O}$ is the molar mass of water (which has a value of $18.018 \times 10^{-3}$ kg mol$^{-1}$).

### 2.1.1. Nernst voltage

The Nernst equation for the reaction described above is given by [4]

$$E_{Nernst} = 1.229 - 0.85 \times 10^{-3}(T_{cell} - 298.15) + 4.3085 \times 10^{-5} T_{cell}(\ln(p_{H_2}^{interface}) + 0.5 \ln(p_{O_2}^{interface})) \tag{6}$$

where $T_{cell}$ is the stack temperature (K), and $p_{H_2}^{interface}$ and $p_{O_2}^{interface}$ are the hydrogen and oxygen partial gas pressures (bar) at the surface of the catalyst at the anode and cathode, respectively.

The partial pressures at the catalyst surface are assumed to be the same across the entire cell, and are given by [2,6]

$$p_{H_2}^{interface} = (0.5 p_{H_2O}^{sat}) \left[ \frac{1}{e^{1.653 i / T_{cell}^{1.334}} x_{H_2O}^{channel}} - 1 \right] \tag{7}$$

and

$$p_{O_2}^{interface} = P_{cell}[1 - x_{H_2O}^{sat} - x_{other\ gases}^{channel} e^{0.291 i / T_{cell}^{0.832}}] \tag{8}$$

where $x_{H_2O}^{sat}$ is the molar fraction of water in a gas stream at saturation for a given temperature, $x_{othergases}^{channel}$ the molar fraction of other gases (apart from oxygen) in the air stream, $p_{H_2O}^{sat}$ the saturation pressure of water vapour at a given temperature, $P_{cell}$ the cell operating pressure, and $i$ is the current density (A cm$^{-2}$). The derivation of Eqs. (7) and (8) is based on the Maxwell–Stefan equations, and the interested reader is referred to Ref. [2] for a more detailed explanation. After assuming that the flux of water vapour and nitrogen (in the cathode) are zero, the Maxwell–Stefan equation becomes a simple ordinary differential equation that can be integrated analytically. The equations are derived by solving this equation, substituting the value of all constants and approximating the diffusion coefficient using kinetic theory. A detailed explanation of how the equations are derived is given in Ref. [2].

The molar fraction of water at saturation in a gas stream for a given temperature is given by

$$x_{H_2O}^{sat} = \frac{p_{H_2O}^{sat}}{P_{cell}} \tag{9}$$

where $P_{cell}$ is the cell operating pressure and the $p_{H_2O}^{sat}$ term is determined in a fuel cell by the following empirical equation [20]

$$\ln(p_{H_2O}^{sat}) = 70.434643 - \frac{7362.6981}{T_{cell}} + 0.006952085 \times T_{cell} - 9.0000 \times \ln T_{cell} \tag{10}$$

The molar fraction of other gases (mostly nitrogen gas) in the air stream is given by a log mean average between the molar fraction of other gases in a humidified stream of air at the inlet and the molar fraction at the outlet [2,21]

$$x_{other\ gases}^{channel} = \frac{x_{other\ gases}^{in,hum} - x_{other\ gases}^{out,hum}}{\ln(x_{other\ gases}^{in,hum} / x_{other\ gases}^{out,hum})} \tag{11}$$

where

$$x_{other\ gases}^{in,hum} = (1 - x_{H_2O}^{sat}) \times 0.79 \tag{12}$$

and

$$x_{other\ gases}^{out,hum} = \frac{1 - x_{H_2O}^{sat}}{1 + (\lambda_{air} - 1/\lambda_{air})(0.21/0.79)} \tag{13}$$

In Eqs. (12) and (13), the 0.79 term refers to the dry molar fraction of other gases in air, while in Eq. (13), the 0.21 term refers to the dry molar fraction of oxygen in air. The $\lambda_{air}$ term denotes the stoichiometry of the air stream.

### 2.1.2. Activation overvoltage

The semi-empirical equation for the activation overvoltage is given by [4]

$$\eta_{act} = \beta_1 + \beta_2 T_{cell} + \beta_3 T_{cell} \ln(C_{O_2}^{interface}) + \beta_4 T_{cell} \ln(I) \tag{14}$$

Table 1
Empirical coefficients for PEMFC stack model

| | $\beta_1$ | $\beta_2$ | $\beta_3$ | $\beta_4$ |
|---|---|---|---|---|
| Amphlett et al. [2] and Xue and Dong [6] for Ballard Mark V stack | −9.514 | 0.00312 | 0.0000740 | −0.000187 |
| Pastula [20] and Wang and Dong [8] for an ambient air PEMFC stack | −0.944 | 0.00354 | 0.0000785 | −0.000196 |
| Mann et al. [4] and Fowler et al. [5] for Ballard Mark IV and V stacks | −0.948 | [a] | 0.000076 | −0.000193 |

[a] $\beta_2 = 0.00286 + 0.0002 \ln A_{\text{active}} + (4.3 \times 10^{-5}) \ln c^*_{H_2}$.

where

$$C_{O_2}^{\text{Interface}} = \frac{p_{O_2}^{\text{interface}}}{5.08 \times 10^6 \, e^{(-498/T_{\text{cell}})}} \tag{15}$$

and where the expression for $p_{O_2}^{\text{interface}}$ is given in Eq. (8) and the $\beta$ coefficients of Eq. (14) are empirically determined for each individual fuel cell stack. Their previously published values are given in Table 1. The values used during this research are contained in the third entry of Table 1. The term $A_{\text{active}}$ in the description of $\beta_2$ is the active area of the fuel cell ($cm^2$), given in Eq. (18).

### 2.1.3. Ohmic overvoltage

The ohmic overvoltage can be expressed in accordance with Ohm's law as [4]

$$\eta_{\text{ohmic}} = \eta_{\text{ohmic}}^{\text{electronic}} + \eta_{\text{ohmic}}^{\text{protonic}} = -i(R^{\text{electronic}} + R^{\text{protonic}}) \tag{16}$$

where $R^{\text{electronic}}$ is assumed to be a constant over the operation temperature of the PEMFC. The electronic resistance is further assumed to be inconsequential in comparison to protonic resistance, and is thus ignored. The term $R^{\text{protonic}}$ is known to be a complex function of water content and distribution in the membrane, which in turn is a function of the cell temperature and current. A general expression for the ohmic resistance of the electrolyte is given by [20]

$$R^{\text{protonic}} = \frac{r_M t}{A_{\text{active}}} \tag{17}$$

where $r_M$ is the membrane-specific resistivity for the flow of hydrated protons ($\Omega$ cm), $t$ the thickness of membrane (cm) and $A_{\text{active}}$ is the active cell area ($cm^2$). Based on the specific fuel cell plate and flowfield design, the active cell area is only a portion of the stack cross-sectional area, at 56% [20]. The other 44% of the area are used to accommodate the rods that hold the stack, the manifolds for hydrogen fuel, oxidant air and coolant, as well as the seals surrounding the parameter of the plate and these manifold holes. This value is stack design dependent, but representative for a PEM stack. The active area is then given by

$$A_{\text{active}} = 0.56 A_t \tag{18}$$

where $A_t$ is the total stack cross-sectional area. While the other two terms in Eq. (17) are known parameters of a specific cell, the term $r_M$ is difficult to describe phenomenologically, and thus the following semi-empirical expression has been derived [5]

$$r_M = \frac{181.6[1 + 0.03(i) + 0.062(T_{\text{cell}}/303)^2 i^{2.5}]}{[\lambda_{\text{membrane}} - 0.634 - 3i] \, e^{3.25(T_{\text{cell}} - 303/T_{\text{cell}})}} \tag{19}$$

where again $i$ is the current density; $\lambda_{\text{membrane}}$ is in this case an adjustable fitting parameter influenced by the method of manufacture of the membrane, and a function of the relative humidity and stoichiometric ratios at the anode and cathode and of the age and use of the membrane. The parameter is usually assigned a value between 10 and 20, and in this case it takes the value of 14.6 [5]. Eq. (19) is developed in Ref. [5] in a semi-empirical manner, based on mechanistic equations found in [22,23] and experimental data at RMC, as explained in [4]. It should be noted that the current version of the model assumes a fully humidified membrane; a membrane hydration module is currently under development.

### 2.1.4. Concentration overvoltage

The expression used in the model for the concentration overvoltage is given by [19]

$$\eta_{\text{conc}} = \frac{RT_{\text{cell}}}{2F} \ln\left(1 - \frac{I}{I_L}\right) \tag{20}$$

where $R$ is the universal gas constant (which has a value of 8.3145 J $mol^{-1}$ $K^{-1}$), $T_{\text{cell}}$ the cell temperature (K), $F$ Faraday's constant (which has a value of 96485.34 C $mol^{-1}$ $electron^{-1}$), $I$ the total current in the fuel cell (A) and $I_L$ is the current (A) at which the hydrogen fuel is used up at a rate that is equal to its supply rate, hence the current $I$ can never be greater than $I_L$. This overvoltage term dominates at higher current densities.

## 2.2. Fuel cell gross output

The gross output of the fuel cell stack ($W$) is given by

$$W_{\text{gross,stack}} = I V_{\text{cell}} n_{\text{cell}} \tag{21}$$

where $n_{\text{cell}}$ is the number of cells in the stack. The number of cells is 27 for this study, as this is the actual number of cells in the physical stack on which testing has taken place. Note that the inclusion of the cell number in the optimization would not yield useful results since there is no penalty for increasing the number of cells; more cells would simply increase the output power and the optimization would determine the upper bound to be the "optimal" choice. If volumetric and system weight considerations were taken into account and the output power decreased with, for example, increased weight, the number of cells in the stack could be included in the optimization.

### 2.2.1. Heat production

Heat is generated by the operation of the fuel cell since the enthalpy that is not converted to electrical energy will instead be converted to thermal energy. This will raise the temperature of the fuel cell beyond its operating temperature range, and must

be addressed using a cooling system. The model in this work assumes that the passage of reactant air through the cell will account for some of the heat transfer, while the cooling system will account for the removal of the remaining excess heat to maintain the proper cell temperature. A fuel cell stack will generate the following amount of heat during operation:

$$\dot{Q}_{\text{total}} = (E_{\max} - V_{\text{cell}})In_{\text{cell}} \tag{22}$$

where $E_{\max}$ is the maximum voltage obtained if the hydrogen 'caloric value', i.e. the heating value or enthalpy of formation were transformed into electrical energy, and is given by

$$E_{\max} = \frac{\Delta H}{nF} = 1.48\,\text{V} \tag{23}$$

where $\Delta H$ is the change in enthalpy.

Heat will be lost to the surroundings and to the air stream through three heat transfer processes: radiation, convection and evaporation. Thus, the amount of heat lost to the air stream and surroundings can be calculated using the following expression:

$$\dot{Q}_{\text{air,total}} = \dot{Q}_{\text{rad}} + \dot{Q}_{\text{conv,total}} + \dot{Q}_{\text{evap}} \tag{24}$$

The amount of heat emitted through radiation by the fuel cell stack to its surroundings is given by

$$\dot{Q}_{\text{rad}} = \sigma A_{\text{cell}}(T_{\text{stack}}^4 - T_0^4) \tag{25}$$

where $\sigma$ is the Stefan–Boltzmann constant (which has a value of $5.67 \times 10^{-8}\,\text{W m}^{-2}\,\text{K}^{-4}$), $T_{\text{stack}}$ is the average temperature the stack (assumed to be the same as $T_{\text{cell}}$), $T_0$ is the ambient air temperature, and $A_{\text{cell}}$ is the area of the radiative stack body, given by

$$A_{\text{cell}} = 0.85 \times 2A_{\text{Ends}} + 0.70 \times 1.3A_{\text{Sides}} \tag{26}$$

where the decimal terms determine the actual surface area of the fuel cell stack. In this model, 85% of the two end plates is the effective heat radiating area, and 70% of the surrounding area of the stack is exposed. The geometry of the stack effectively increased the heat radiating area by 30%, leading to a coefficient of 1.3. The heat loss due to convection will occur differently for the various parts of the fuel cell interior. The convection lost by the vertical walls of the cell is given by [21]

$$\dot{Q}_{\text{conv,walls}} = 1.15A_{\text{Sides}}h_{\text{conv}}(T_{\text{stack}} - T_0) \tag{27}$$

where $h_{\text{conv}}$ is the heat transfer coefficient of the cell channel sides ($\text{W m}^{-2}\,\text{K}^{-4}$), and is calculated using Eq. (28) [20]. The coefficient 1.15 also incorporates the effective side area of the stack based on the non-smooth stack geometry. The heat transfer coefficient is given by

$$h_{\text{conv}} = \frac{k_{\text{air}}Nu}{l} \tag{28}$$

where $k_{\text{air}}$ is the thermal conductivity of air ($\text{W m}^{-2}\,\text{K}^{-4}$), $Nu$ the dimensionless Nusselt number and $l$ is the stack length. The heat transfer due to convection on the top and bottom of the channel is given by [21]

$$\dot{Q}_{\text{conv,top+bottom}} = (h_{\text{conv,top}} + h_{\text{conv,bottom}})(T_{\text{stack}} - T_0)A_{\text{ends}} \tag{29}$$

where $h_{\text{conv,top}}$ and $h_{\text{conv,bottom}}$ are the heat transfer coefficients due to convection of the top and bottom of the fuel cell channel, respectively. The total heat lost to convection is then given by the sum of Eqs. (27) and (29):

$$\dot{Q}_{\text{conv,total}} = \dot{Q}_{\text{conv,walls}} + \dot{Q}_{\text{conv,top+bottom}} \tag{30}$$

The model calculates the amount of heat lost to evaporation, using an assumption that 90% of the water produced is evaporated. Further research is to be carried out to confirm this assumption. The amount of heat required to convert a mass of liquid water to vapour water is equal to the product of the latent heat of vaporization $l_{\text{vap}}$ and the mass of the water. An expression for the amount of heat lost to evaporation is given as [21]

$$\dot{Q}_{\text{evap}} = l_{\text{vap}}0.90\dot{m}_{\text{H}_2\text{O,produced}} \tag{31}$$

where the equation for water production was given in Eq. (5).

### 2.3. Parasitic power considerations

Several auxiliary systems, known as the balance of plant (BOP), are necessary for the correct operation of a fuel cell system. The most important auxiliary systems are the air compressor necessary to pressurize the oxidant air to the correct fuel cell operating pressure; the humidifier to guarantee that the fuel cells are properly humidified for optimal performance; and the cooling system to maintain the cell temperature. All of these auxiliary systems are listed and a representative model for each is described in the following sections.

The BOP components will draw power from that produced by the fuel cell, thereby reducing the overall power output. The total parasitic power of the fuel cell stack is modeled by the equation:

$$W_{\text{net,parasitic}} = W_{\text{cool,pump}} + W_{\text{humid,pump}} + W_{\text{compressor}} \tag{32}$$

Approximately, 80% of the total heat produced will be carried away by the cooling system; the rest of the heat will be removed by the reactant air. The power (W) required to pump the coolant water is given as [20]

$$W_{\text{cool,pump}} = \frac{\dot{m}_{\text{H}_2\text{O}}}{\rho_{\text{H}_2\text{O}}} P_{\text{drop,coolant}} \frac{S_{\text{Factor}}}{\eta_{\text{pump}}\eta_{\text{motor}}} \tag{33}$$

where $S_{\text{Factor}}$ is a factor of safety (assigned a value of 1.5) to account for any pressure losses that are not considered explicitly, $P_{\text{drop,coolant}}$ is the pressure drop of the coolant through the coolant loop, and $\eta_{\text{pump}}$ and $\eta_{\text{motor}}$ are the efficiencies of the pump and motor, respectively. The assumptions have been made in the model that there is a pressure drop of the coolant water through the system of $1 \times 10^4$ Pa and that the efficiencies for the pump and pump motor are 60% and 80%, respectively. The mass of water ($\text{kg s}^{-1}$) required to perform the heat transfer to the water coolant is [20]

$$\dot{m}_{\text{cool,H}_2\text{O}} = \frac{\dot{Q}_{\text{total}} - \dot{Q}_{\text{air,total}}}{c_{p_{\text{H}_2\text{O}}}(T_{\text{stack}} - T_{\text{cool,H}_2\text{O,in}})} \tag{34}$$

where $c_{p_{\text{H}_2\text{O}}}$ is the specific heat of water at constant pressure and $T_{\text{cool,H}_2\text{O,in}}$ is the temperature of the coolant water at the inlet of the stack.

Operation of the humidifier pump also contributes to the power loss. The total humidifier power consumed is given by

$$W_{\text{humid,pump}} = \frac{\dot{m}_{\text{H}_2\text{O,produced}}}{\rho_{\text{water}}} P_{\text{drop,humid}} \frac{S_{\text{Factor}}}{\eta_{\text{pump}}\eta_{\text{motor}}} \tag{35}$$

The model implementations then assume that the pressure drop in the humidifier to be $1 \times 10^5$ Pa and that the pump and motor efficiencies are the same as for the cooling system. The amount of water necessary to fully humidify the hydrogen is [24]

$$\dot{m}_{\text{H}_2\text{O,in H}_2} = \frac{8.937 p^{\text{sat}}_{\text{H}_2\text{O}}}{P_{\text{cell}} - p^{\text{sat}}_{\text{H}_2\text{O}}} \dot{m}_{\text{H}_2} \tag{36}$$

where $\dot{m}_{\text{H}_2}$ is the mass flow of hydrogen gas, given by

$$\dot{m}_{\text{H}_2} = \dot{N}_{\text{H}_2} M_{\text{H}_2} \tag{37}$$

and $M_{\text{H}_2}$ is the molar mass of hydrogen ($2.016 \times 10^{-3}$ kg mol$^{-1}$).

Similarly, the amount of water injected into the air stream is given by

$$\dot{m}_{\text{H}_2\text{O,in air}} = \frac{0.6219 p^{\text{sat}}_{\text{H}_2\text{O}}}{P_{\text{cell}} - p^{\text{sat}}_{\text{H}_2\text{O}}} \dot{m}_{\text{air}} \tag{38}$$

where $\dot{m}_{\text{air}}$ is the mass flow of the reactant air, given by

$$\dot{m}_{\text{air}} = \dot{N}_{\text{O}_2} M_{\text{air}} \tag{39}$$

where $M_{\text{air}}$ is the molar mass of air ($28.97 \times 10^{-3}$ kg mol$^{-1}$). The amount of water passing through the heat exchanger is thus

$$\dot{m}_{\text{H}_2\text{O,heat exchanger}} = \dot{m}_{\text{H}_2\text{O,produced}} - \dot{m}_{\text{H}_2\text{O,in H}_2} - \dot{m}_{\text{H}_2\text{O,in air}} \tag{40}$$

Proof of the connections to phenomenologically based theory for Eqs. (35)–(38) has not yet been fully established, and the equations should be studied in detail in the future to determine their accuracies.

A compressor is required only for the cathode side of the fuel cell since the hydrogen gas is assumed to be stored in a pressurized container. The expression for the compressor power is given as [19]

$$W_{\text{compressor}} = c_{p_{\text{air}}} \dot{m}_{\text{air}} \frac{T_{\text{air,in}}}{\eta_{\text{comp}}} \left( \left( \frac{P_{\text{cell}}}{P_{\text{air,atm}}} \right)^{\gamma - 1/\gamma} - 1 \right) \tag{41}$$

where $c_{p_{\text{air}}}$ is the specific heat of air that varies with temperature, $\gamma$ is the isentropic compression ratio, or Cp/Cv, and is calculated from the ratio of operation pressure $P_{\text{cell}}$ to atmospheric pressure, the compressor efficiency is assigned a value of 60%, and $P_{\text{air,atm}}$ is atmospheric pressure.

### 2.4. System net output and efficiency

The net system power output is the gross output power of the stack, given in Eq. (21), subtracted by the total parasitic power, calculated in Eq. (32):

$$W_{\text{net,system}} = W_{\text{gross,stack}} - W_{\text{net,parasitic}} \tag{42}$$

The system energy efficiency, also known as first law efficiency, is calculated using the equation [22]:

$$\eta_{\text{system,energy}} = \frac{W_{\text{net,system}}}{\sum_{\text{in}} \dot{N}_{\text{react},i} h_{\text{react},i} - \sum_{\text{out}} \dot{N}_{\text{prod},j} h_{\text{prod},j}} \tag{43}$$

where $\dot{N}_{\text{react},i}$ is the molar flow (mol s$^{-1}$) and $h_{\text{react,i}}$ the enthalpy (kJ mol$^{-1}$) of a reactant of the electrochemical reaction taking place in the fuel cell stack and $\dot{N}_{\text{prod},j}$ is the molar flow (mol s$^{-1}$) and $h_{\text{prod},j}$ is the enthalpy (kJ mol$^{-1}$) of a product. The inlet molar mass flow of $H_2$ was given in Eq. (3). The enthalpy terms of Eq. (43) are calculated using thermodynamic tables and depend only on temperature for the gases (assumed ideal) and on the temperature and enthalpy of formation for the liquid water formed at the cathode.

The stoichiometry of hydrogen in this study is set to be 1.1 and the outlet molar flow of $H_2$ (mol s$^{-1}$) is given by the subtraction of the usage from the supply:

$$\dot{N}_{\text{H}_2,\text{out}} = \dot{N}_{\text{H}_2,\text{in}} - \frac{In_{\text{cell}}}{2F} = \frac{In_{\text{cell}}}{2F}(\lambda_{\text{H}_2} - 1) = 0.1 \frac{In_{\text{cell}}}{2F} \tag{44}$$

Again, a similar expression can be found for the oxygen at the outlet of the stack.

Another more useful metric for measuring the stack performance is the exergetic efficiency since it provides a true analysis of the irreversibilities of the system that the energy efficiency does not capture. The exergetic efficiency is also known as the second law efficiency. The equation for the system exergetic efficiency is given by [25]

$$\eta_{\text{system,exergetic}} = \frac{W_{\text{net,system}}}{\sum_{\text{in}} \dot{N}_{\text{react},i} \xi_{\text{react},i} - \sum_{\text{out}} \dot{N}_{\text{prod},j} \xi_{\text{prod},j} - \dot{Q}_{\text{exit}}(1 - T_0/T_{\text{stack}})} \tag{45}$$

where $\xi_{\text{react},i}$ is the exergy (also known as the availability) of a reactant $i$ flowing into the system, $\xi_{\text{prod},j}$ is the exergy of a product $j$ flowing out of the system, $\dot{Q}_{\text{exit}}$ is the heat leaving the stack (and used to heat the air and release the hydrogen if a metal hydride hydrogen storage device, instead of a compressed hydrogen tank, is used as the onboard fuel storage means), $T_0$ is the ambient air temperature, and $T_{\text{stack}}$ is the stack operating temperature (equal to $T_{\text{cell}}$). The only reactant containing exergy is actually the hydrogen stream; the product hydrogen, oxygen, nitrogen and water exiting the system will all possess exergy. The exergy of a substance (kJ kmol$^{-1}$) is given by [26]

$$\xi = \xi_{\text{KE}} + \xi_{\text{PE}} + \xi_{\text{TM}} + \xi_{\text{CH}} \tag{46}$$

where $\xi_{\text{KE}}$, $\xi_{\text{PE}}$, $\xi_{\text{TM}}$, and $\xi_{\text{CH}}$ are the exergies due to an imbalance of the substance with the reference kinetic energy, potential energy, thermomechanical, and chemical equilibrium point, respectively. The first two terms are assumed to be negligible, and the latter two terms are defined by [23]

$$\xi_{\text{TM}} = (h - h_0) - T_0(s - s_0),$$
$$\xi_{\text{CH}} = \sum_j x_j(\mu_{j0} - \mu_{j00}) \tag{47}$$

where $h$, $s$, and $\mu_j$ denote the specific enthalpy, entropy, and chemical potential of substance $j$, respectively, at a given state, and $x_j$ is the molar fraction of substance $j$. The subscript 0 in the first equation indicates that the property is associated with the reference environmental (restricted) state where pressure and temperature are at equilibrium. The double subscript in the second equation refers to the dead state where pressure, temperature and chemical potential are at equilibrium.

## 3. PEMFC stack and empirical parameters

The stack used for the study is based on the Palcan PC6-1200, which is a PEMFC stack, comprised of 25 adjacent cells in a conventional plate-and-frame arrangement with volumetric dimensions of approximately 15 cm × 19 cm × 21 cm, and its total active area is 96 $cm^2$. The weight of the stack is approximately 1.5 kg. Inlet and exhaust ports for fuel, oxidant and water are accessible from both ends of the stack for installation versatility and convenience. The designed minimum operating conditions of the PC6 stack are pressures slightly above atmospheric (3 psi gauge, or 0.21 bar gauge) and a temperature of 45 °C average. The maximum gross power output of the stack (and system) is 1200 W. The empirical coefficients for the Mark V PEMFC stack model, given in the last row of the three entries in Table 1, are used in this study. Extensive stack tests on the Palcan PEMFC stack have been carried out, and the new parameter models resulting from these tests will be presented in subsequent work.

## 4. System optimization

The design of a PEMFC system often involves several conflicting objectives. In this case, the power consumed by the auxiliary systems creates several conflicts of interest when the net output power is to be maximized. The operation of the fuel cell is ameliorated significantly at a high temperature and pressure; however, these increases would result in higher power losses due to the auxiliary systems, in particular due to the cooling system and the air compressor, respectively. It is because of these conflicting interests that the design of a fuel cell system is a good candidate for optimization.

To solve the optimization problem posed by the conflicting goals in the fuel cell system three popular and successful optimization techniques have been chosen: (1) simulated annealing (SA); (2) genetic algorithm (GA); (3) sequential quadratic programming (SQP). The first two are global optimization algorithms, while the third is a local optimization algorithm. The global optimization algorithms are used to ensure that the global minimum is determined in the optimization. The local optimization algorithm is chosen to gain some insight into the objective function for this type of problem. If the SQP algorithm does not produce results similar to those of the global optimization methods, then it is clear that the objective function is not unimodal and smooth, but in fact contains local minima, which "trapped" the local optimization algorithm.

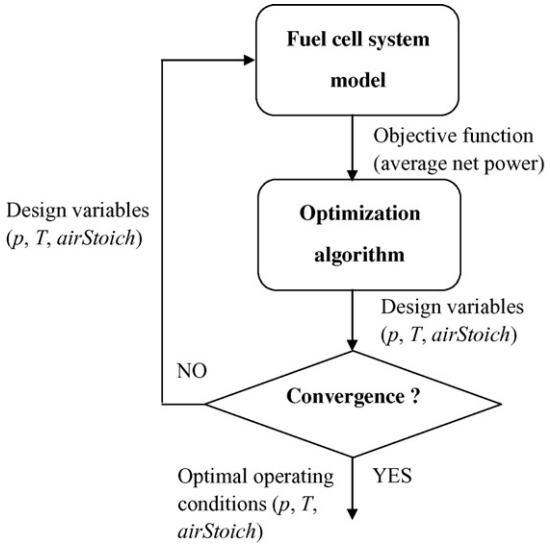


Fig. 2. Flow diagram of the optimization program.

To solve the optimization problem the fuel cell system model described in the previous section is coupled to the optimization algorithms described above as shown in Fig. 2 for the case of average net power optimization. The coupling between the optimization algorithm and the model is achieved through the design variables and the objective function and constraints. First, the optimization algorithm or the user selects the initial value for the design variables and the objective function. In the case of global methods, the initial value for the design variables is selected randomly. In the case of a local method, the user gives the initial value for the design variables. The value of the design variables is then given to the fuel cell system model. The fuel cell system model then computes the performance of the system, and from those results computes the value of the objective function subject to the design constraints. With this information, the optimization algorithm chooses a new set of design variables that can potentially increase the system performance. This process is repeated until a convergence criterion is satisfied or the maximum number of iterations is achieved, depending on the optimization algorithm used.

Finally, if a local optimization algorithm is used for optimization, the gradients are computed using adaptive forward differences. In this case, the optimization algorithm automatically calls the fuel cell system model with a small perturbation in each one of the design variables and computes the numerical gradient.

## 5. Discussion and results

The fuel cell system model and the optimization methods described above are used to optimize the operating conditions of a fuel cell system for two different applications: vehicular and stationary. In both optimization problems, two optimizations are performed with different objectives: the maximization of the net power and of the system exergetic efficiency.

### 5.1. Vehicular application—a multi-objective optimization problem

One of today's most important applications of PEM fuel cell system is to serve as the powerplant for an electric or hybrid vehicle. In this application, the fuel cell system needs to operate over a wide range of power requirements, and the power demands on the fuel cell system change with varying levels of acceleration and velocity. Therefore, it is desired to obtain the fuel cell system operating conditions that yield the maximum net power or exergetic efficiency over varying power demands to maximize acceleration and velocity or vehicle range performance, respectively. The fuel cell system design optimization problem is then formulated as a multi-objective optimization problem:

$$\begin{aligned} &\underset{\text{w.r.t. } \mathbf{x}}{\text{maximize}}: \quad f(\mathbf{x}, i) = \sum_{j=1}^{N} w_j W_j(\mathbf{x}, i_j) \\ &\text{subject to}: \quad \mathbf{x}_{\max} \geq \mathbf{x} \geq \mathbf{x}_{\min} \end{aligned} \tag{48}$$

or

$$\begin{aligned} &\underset{\text{w.r.t. } \mathbf{x}}{\text{maximize}}: \quad f(\mathbf{x}, i) = \sum_{j=1}^{N} w_j \eta_j(\mathbf{x}, i_j) \\ &\text{subject to}: \quad \mathbf{x}_{\max} \geq \mathbf{x} \geq \mathbf{x}_{\min} \end{aligned} \tag{49}$$

where $W_j(\mathbf{x}, i_j)$ is the net power and $\eta_j(\mathbf{x}, i_j)$ the system exergetic efficiency obtained from the fuel cell system at a current density $i_j$ for objective $j$, $w_j$ the weighting of objective $j$, and $\mathbf{x}$ is the vector of design variables. The net power output and exergetic efficiency of the fuel cell system is obtained using the computational model described above. The design variables include the operating temperature, the air stoichiometry, and the operating pressure of the fuel cell stack. The upper and lower limits of these design variables are $\mathbf{x}_{\max}$=[373, 5, 15] and $\mathbf{x}_{\min}$ = [338, 1.5, 1], respectively. If only two objectives were present, it would be possible to create a Pareto curve to see the trade-off between objectives; in this case, however, the objectives are the maximization of the average net power and average exergetic efficiency for every value of current density from 0.1 to 1.3 A cm$^{-2}$. The multi-objective optimization problem with different weights will yield different optimal operating conditions. The weights are used in order to give equal importance to the power or efficiency at all current densities. This is achieved by using the weights to normalize the power or exergy at each current density.

The maximization of the net power is solved using the three-optimization algorithms described above and the results are provided in Table 2. The solutions of the three methods are almost identical. Only the solution achieved using the GA has a small error and increasing the number of generations in the algorithm will reduce this error. The SA algorithm stopped when a convergence criterion of three successive iterations with a difference in the objective function smaller than $1 \times 10^{-6}$ was satisfied. The GA algorithm stopped after running 200 generations; the convergence criterion was not specified. Finally, the SQP algorithm stopped when the module of the gradient of the objective function reached a value less than $1 \times 10^{-8}$. In principle, the solution of the SQP is dependent on the given initial point. The results were obtained from a variety of different initial points and the same solution was achieved in the calculations.

Due to the different nature of the methods and the different convergence criteria it is difficult to do a thorough comparison of the computational expense of these methods. Looking at the number of function evaluations and the required computational time in Table 2 for the three methods, we can observe that the local method (SQP) converges to the solution very quickly, and similar results were obtained when the initial starting point was varied. From this assessment, it can be observed that the shape of the objective function is likely to be smooth and convex (unimodal) since the local method converges to the same solution regardless of the choice for the initial point.

In order to be able to show the improvements given by the new operating conditions, the performance of the fuel cell system is compared to the performance of the same fuel cell at nominal operating conditions. The fuel cell system running at the nominal operating condition is known as the base case in the rest of the paper. The base operating conditions include a temperature of 355 K, hydrogen and air stoichiometry ratios of 1.1 and 2.5, respectively, and a pressure of 3 bar. Then, performances of the fuel cell system operating at the calculated optimal operating conditions and at base operating conditions are compared. The differences between the base and optimized operating conditions were: 3.2% (temperature); −40% (air stoichiometry); −31.9% (pressure).

Fig. 3 depicts the net output power of the fuel cell system at the optimal and base operating conditions. A large increase in the net output power can be observed, with the optimal peak at 932.74 W and the base peak at 728.36 W, a significant increase of 21.9%. This increase in net power is due to a decrease in the necessary power of the auxiliary devices since the gross output power between the base and optimized operating conditions is similar, as shown in Fig. 4. The optimization has also moved the point at which maximum net power is achieved to a higher current density, from 0.89 to 1.007 A cm$^{-2}$, a change of 11.6%.

At the base operating conditions and at an arbitrary current density of 0.76 A cm$^{-2}$, the consumed powers in the cooling

Table 2
Solution of the multi-objective problem (net power optimization)

| Optimization algorithm | Objective function: average net power (W) | Solution: {$T$(K), AirStoich, $P$ (bar)} | Number of function evaluations | CPU time (s) |
|---|---|---|---|---|
| Simulated annealing | 663.68 | {366.84, 1.500, 2.043} | 3001 | 55.1 |
| Genetic algorithms | 663.80 | {366.41, 1.500, 2.011} | 4000 | 615.8 |
| SQP | 663.68 | {366.84, 1.500, 2.043} | 100 | 3.0 |

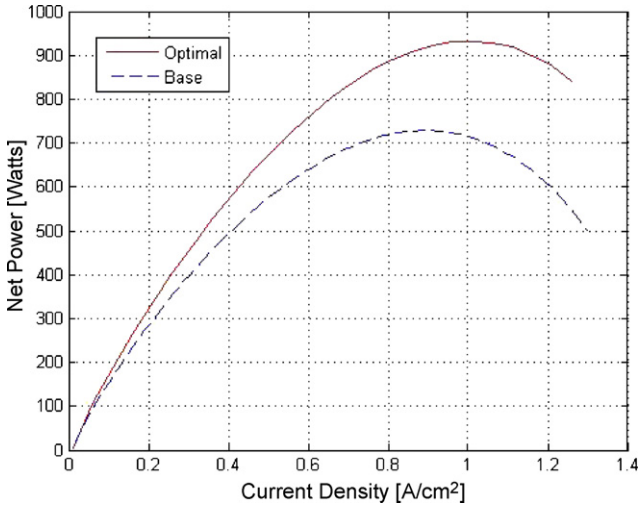


Fig. 3. Net output power of the fuel cell system vs. current density under optimal and base operating conditions.

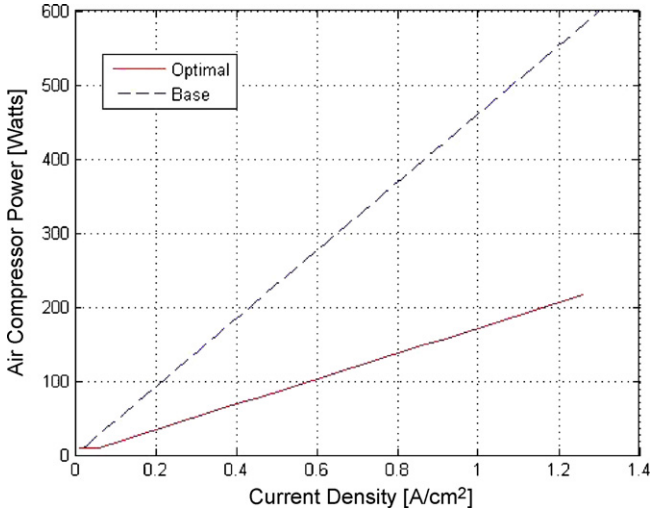


Fig. 5. Consumed power by the air compressor vs. current density under optimal and base operating conditions.

pump, humidifier pump and air compressor are 5.0 W, 5.0 W (minimum allowed power) and 350.1 W, respectively. At the optimal operating conditions and identical current density, the cooling pump, humidifier pump and air compressor consume powers of 5.0, 5.0 and 130.4 W, respectively. This represents decreases of 0%, 0%, and 62.8% in the power consumption of each parasitic device. The parasitic powers of the cooling and humidifier pumps are unchanged since 5.0 W is defined as the minimum power draw of the devices, and both the base case and optimal solution show that this is more than sufficient power to fulfill the cooling and humidification requirements. The large increase in net power is mainly due to the massive reduction in the power consumed by the air compressor, caused by a large reduction in the air stoichiometric ratio and operating pressure. The compressor power is reduced dramatically at all current densities, as shown in Fig. 5.

The efficiency of the fuel cell system is also dramatically improved by the optimization. Fig. 6 illustrates the energy efficiency as a function of current density for both the optimal and base cases, while Fig. 7 depicts the exergetic efficiency as a function of current density. Both figures demonstrate that significant efficiency improvement has been achieved. The peak energy efficiency is 0.475 and the peak exergetic efficiency is 0.700 (both at 0.06 A $cm^{-2}$) for the optimized operating conditions, while the peak energy efficiency is 0.425 (at 0.05 A $cm^{-2}$) and peak exergetic efficiency is 0.648 (at 0.06 A $cm^{-2}$) for the base case, for percent improvements of 10.5% and 7.4%, respectively.

It is also possible and interesting to see the difference in performance when the design objective is to maximize the system efficiency. The optimization results when the objective function is the average exergetic efficiency are included in Table 3.

In this different design optimization problem, the maximum average net system efficiency obtained was 0.515. The peak value of 0.702 (at 0.11 A $cm^{-2}$) is slightly higher than in the previous average net power optimization by 0.3%; more importantly, however, the current density at which the peak exergetic

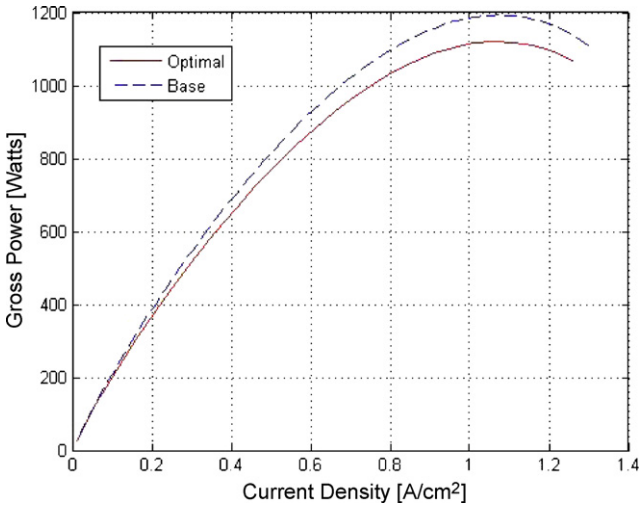


Fig. 4. Gross power output of the fuel cell stack vs. current density under base optimal and base operating conditions.

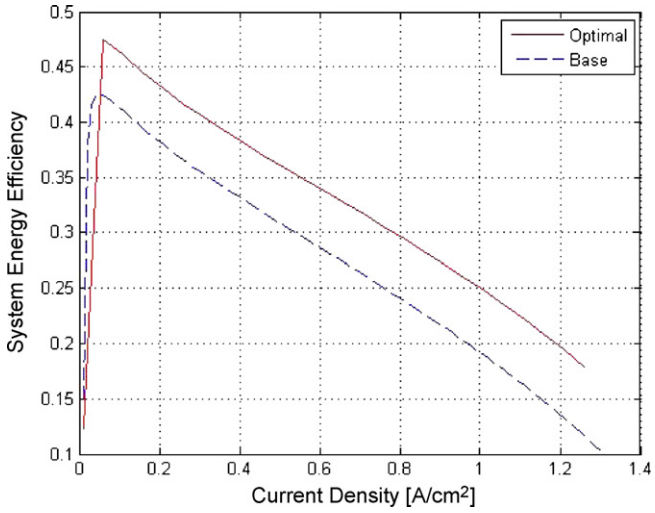


Fig. 6. System energy efficiency vs. current density under optimal and base operating conditions.

Table 3
Solution of the multi-objective problem (exergetic efficiency optimization)

| Optimization algorithm | Objective function: average exergetic efficiency | Solution: {$T$ (K), AirStoich, $P$ (bar)} | Number of function evaluations | CPU time (s) |
|---|---|---|---|---|
| Simulated annealing | 0.515 | {360.72, 5.000, 1.036} | 3301 | 23.4 |
| Genetic algorithms | 0.515 | {360.72, 5.000, 1.036} | 4000 | 306.9 |
| SQP | 0.515 | {360.72, 5.000, 1.036} | 189 | 3.7 |

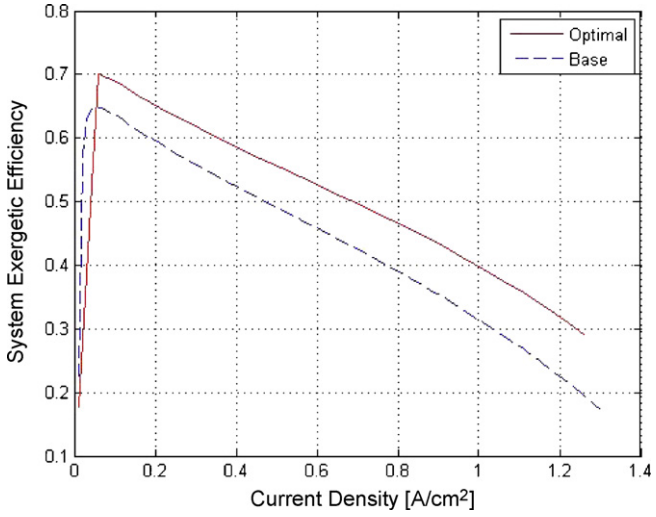


Fig. 7. System exergetic efficiency vs. current density under optimal and base operating conditions.

efficiency is achieved is at a higher, more useful level. The exergetic efficiency as a function of current density is shown below in Fig. 8. The peak net system power is 920.16 (at 1.01 A cm$^{-2}$), which is 1.3% lower than in the case of average net system power optimization. An optimization of the exergetic efficiency of a system is useful because it can directly contribute to lower initial investment and operating costs. The shortage of maximum average power can be addressed by using a hybrid power system with a battery or ultracapacitor to boost the system power when required.

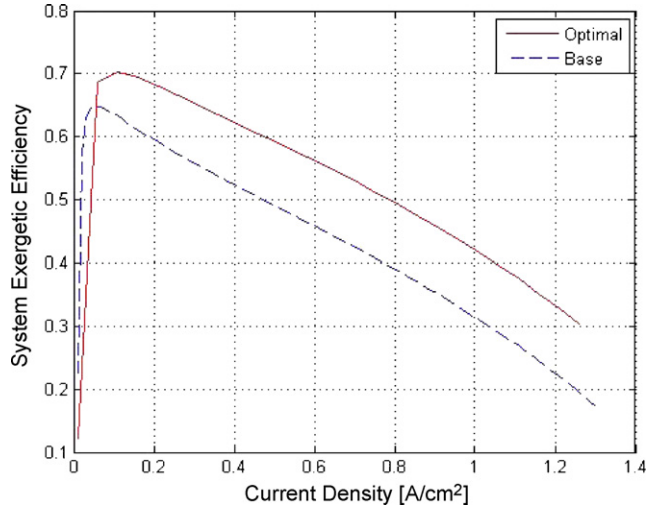


Fig. 8. System exergetic efficiency vs. current density under optimal and base operating conditions (exergetic efficiency optimization).

### 5.2. *Stationary power generation application—a single-objective optimization problem*

Another important application of PEM fuel cell systems is to serve as the power plant for a mobile or stationary power unit to provide stable power supply. In this case, the fuel cell system is to be operated at either the maximum net power or point of maximum exergetic efficiency. For the simple power generation application, it is possible to maintain the fuel cell system at a single operating point. Therefore, the fuel cell operating conditions and the current density that yields the maximum net power or maximum exergetic efficiency are to be obtained. The optimization problem can be formulated as

$$\begin{aligned} &\underset{\text{w.r.t. } \mathbf{x}}{\text{maximize}}: \quad f(\mathbf{x}) = W(\mathbf{x}) \\ &\text{subject to}: \quad \mathbf{x}_{\max} \geq \mathbf{x} \geq \mathbf{x}_{\min} \end{aligned} \tag{50}$$

$$\begin{aligned} &\underset{\text{w.r.t. } \mathbf{x}}{\text{maximize}}: \quad f(\mathbf{x}) = \eta(\mathbf{x}) \\ &\text{subject to}: \quad \mathbf{x}_{\max} \geq \mathbf{x} \geq \mathbf{x}_{\min} \end{aligned} \tag{51}$$

where $W(\mathbf{x})$ is the net power; $\eta(\mathbf{x})$ is the system exergetic efficiency; $\mathbf{x}$ is the design variable vector that includes the operating temperature, air stoichiometry, operating pressure of the fuel cell stack, and current density at which the fuel cell system will operate to achieve maximum net power. The upper and lower limits of the design variables are defined as $\mathbf{x}_{\min} = [338, 1.5, 1, 0.1]$ and $\mathbf{x}_{\max} = [373, 5, 15, 1.3]$.

This problem is also solved using the three-optimization algorithms described and the solutions are presented in Table 4. Furthermore, two initial design points were used to solve the problem using the local method. For SQP-1, $\mathbf{x}_0 = [353, 2.5, 3, 0.75]$ and for SQP-2, $\mathbf{x}_0 = [353, 2.5, 1, 0.75]$.

In this case, there are two different solutions with widely varying operating conditions found by the global and local algorithms, although there is again a small discrepancy observed between the solution obtained using the GA and SA optimization methods, even though they in effect found the same solution. As in the previous case, an increase in the number of generations or the population in GA would likely result in a better result at the expense of a longer computation time. The existence of two distinct solutions suggests that the objective function is non-unimodal. One solution, located by the local SQP-1 algorithm, is at a very high temperature and high pressure with low air stoichiometry (the minimum value is reached); the other solution,

Table 4
Optimal solution of the single-objective problem (net power optimization)

| Optimization algorithm | Objective function: maximum net power (W) | Solution: {$T$ (K), AirStoich, $P$ (bar), $i$ (A/cm$^2$)} | Number of function evaluations | CPU time (s) |
|---|---|---|---|---|
| Simulated annealing | 935.12 | {353.21, 5.000, 1.028, 0.984} | 4401 | 7.8 |
| Genetic algorithms | 934.65 | {353.33, 4.578, 1.029, 0.982} | 4000 | 92.6 |
| SQP-1 | 933.53 | {368.17, 1.500, 1.952, 1.007} | 140 | 0.2 |
| SQP-2 | 935.12 | {353.21, 5.000, 1.028, 0.984} | 244 | 0.3 |

found by both global algorithms and the SQP algorithm with a different initial starting point, is at a much lower temperature and pressure, but with a high air stoichiometry (the maximum value is reached).

The operating conditions for the solution located by the SQP algorithm (SQP-1) are similar to the solution of the multi-objective function problem, although a distinction between the two results is obvious. The optimal temperature is greater for the stationary application than for the vehicular application, while the optimal operating pressure is less. The optimal air stoichiometry is the same for both applications, at the lower bound of the design variable limits. The difference between the maximized net power curves shows that a slight compromise was required between the performances at high and low current densities for the multi-objective optimization problem: the peak net system power for the multi-objective problem is 0.08% less than the peak net system power determined for the single-objective problem.

Fig. 9 shows a curve of the maximum net output power with respect to the current density at the base and optimal operating conditions for the solution found by the SQP-1 algorithm. The peak of the optimized net system power curve is denoted by the small (black) circle at the maximum value. It is interesting to note that the maximum net power is achieved at the same current density, 1.007 A cm$^{-2}$, for which the maximum average net power was determined in the multi-objective problem. The gross power curves are shown in Fig. 10.

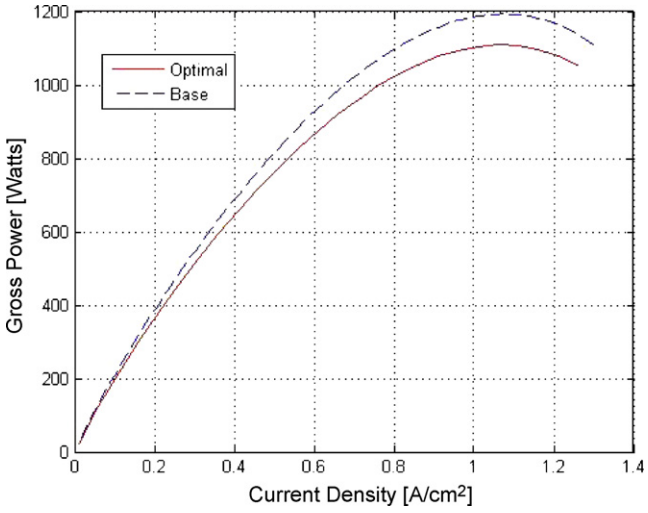


Fig. 10. Gross power output of the fuel cell stack vs. current density under base optimal and base operating conditions (SQP-1 algorithm).

Figs. 11 and 12 depict the net and gross system power for the global algorithms' solution. The net power curve is essentially the same as that for the SQP-1 algorithm, with slight differences in peak net power values and current density at which the peak net power is achieved. However, the gross power curve is quite different showing that the gross power of the fuel cell stack has been reduced significantly, due to the large reduction on the operating pressure and temperature. Even though the gross

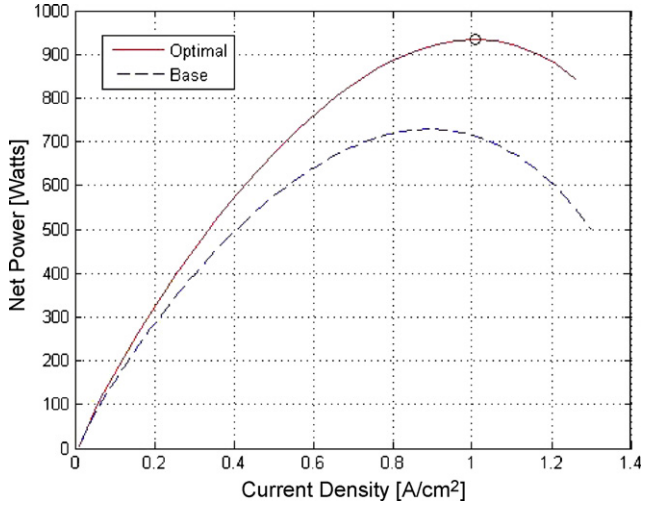


Fig. 9. Fuel cell system net output power vs. current density with peak power shown (SQP-1 algorithm).

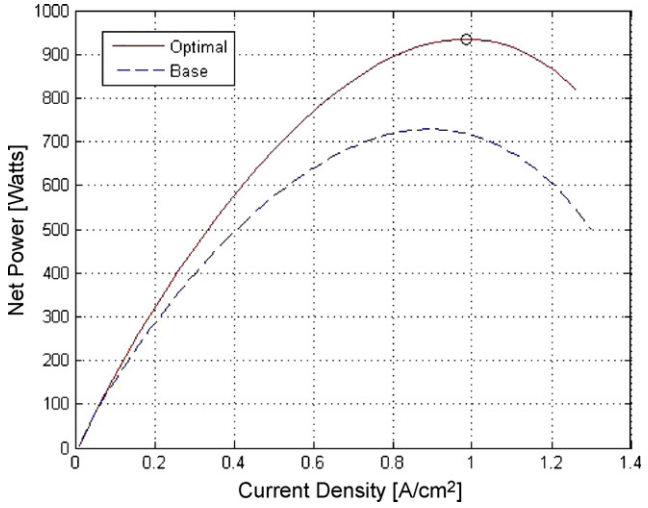


Fig. 11. Fuel cell system net output power vs. current density with peak power shown (global algorithm).

Table 5
Optimal solution of the single-objective problem (system exergetic efficiency)

| Optimization algorithm | Objective function: maximum exergetic efficiency (W) | Solution: {$T$ (K), AirStoich, $P$ (bar), $i$ (A/cm$^2$)} | Number of function evaluations | CPU time (s) |
|---|---|---|---|---|
| Simulated annealing | 0.729 | {363.13, 5.000, 1.158, 0.100} | 4401 | 5.3 |
| Genetic algorithms | 0.729 | {363.31, 4.997, 1.159, 0.100} | 4000 | 64.8 |
| SQP | 0.722 | {361.23, 4.623, 1.175, 0.100} | 506 | 0.8 |

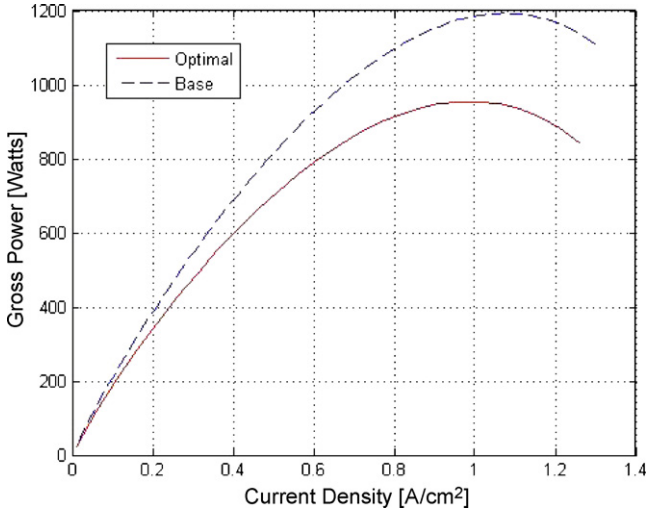


Fig. 12. Gross power output of the fuel cell stack vs. current density under base optimal and base operating conditions (global algorithm).

power is reduced, the increase in net power can be explained by looking at Fig. 13, which shows the compressor power for the global algorithms' solution. When contrasted with the compressor power curve of Fig. 5, a dramatic reduction in power can be easily observed. This reduction in compressor power is mainly due to the reduction of the pressure ratio in Eq. (41). As the pressure ratio tends to one the compressor power goes to zero. This proves that there is a large penalty for increasing the cathode pressure of the fuel cell stack.

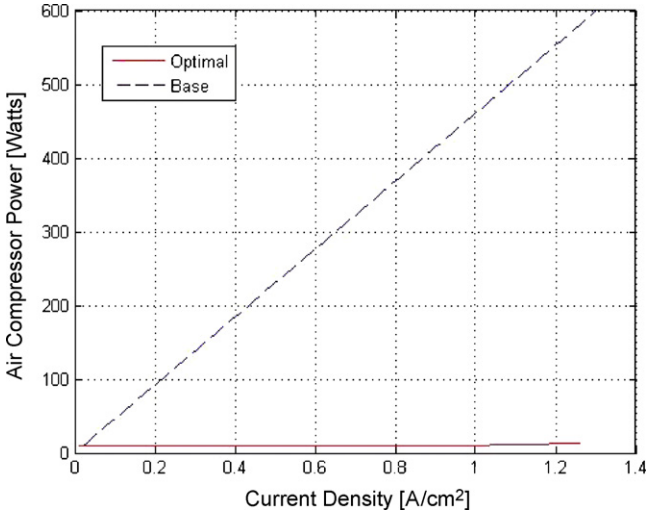


Fig. 13. Consumed power by the air compressor vs. current density under optimal and base operating conditions (global algorithm).

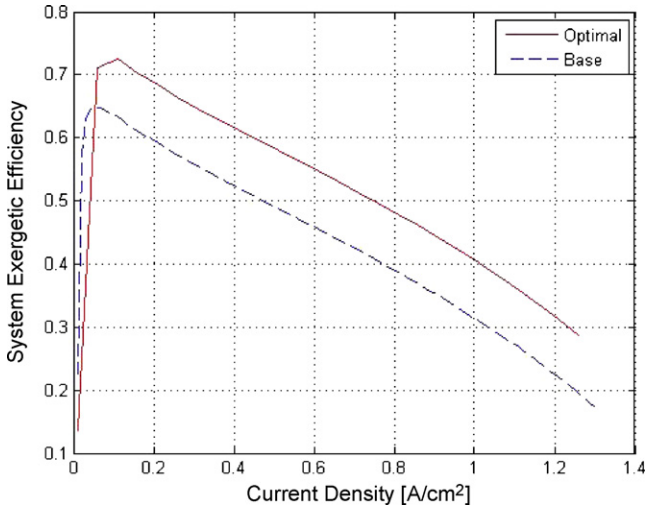


Fig. 14. System exergetic efficiency vs. current density under optimal and base operating conditions for exergetic efficiency optimization.

As in the previous multi-objective optimization problem, the system exergetic efficiency is optimized. The results of the optimization process are depicted below in Table 5.

The maximum peak exergetic efficiency was 0.729, which is an increase from the previous single-objective of 4.0% and 4.3% for the low and high stoichiometry solutions, respectively. The peak of the net system power fell below that of the previously optimized average to 868.81 W (at 0.96 A cm$^{-2}$), although it remained higher than that of the base operating case. The exergetic efficiency curve as a function of the current density is shown in Fig. 14. As stated previously, the maximization of the system exergetic efficiency rather than the net system power can reduce the overall costs of the system, and the shortfall in power can be mitigated through the introduction of a battery or ultracapacitor in a hybridization scheme.

## 6. Conclusions

In this paper, a methodology to obtain the optimal operating conditions for a fuel cell system is outlined. In order to show the validity of the approach, the operating conditions for a fuel cell system employed in two different applications is shown. The new operating conditions improve the net output power or the exergetic efficiency with respect to the nominal or common operating conditions of the system for both applications, demonstrating the usefulness of the approach.

During the study, global and local optimization algorithms were compared. For the multi-objective problem, similar results are obtained using both methods. This allows us to conclude that

this optimization problem has an objective function that is both convex and unimodal. However, the addition of design variables and constraints may change the nature of the problem, and the use of local methods may not be possible. In this particular case, the use of a local optimization technique is preferred since its application results in the same solution as the global methods using less computational time. For the single-objective optimization problem, the differing results of the two methods suggest that the objective function is in this case non-unimodal with at least one local maxima in addition to the global maximum value. Furthermore, the benefit of using both method types is demonstrated by the large variance in operating conditions revealed by the solutions: in practice, one maximum, although at a slightly lower value, may actually be the superior choice. This interesting result suggests that it is prudent to continue to employ both types of algorithms in tandem during any optimization, if possible.

This work reveals a large number of possible avenues of future research. The existing fuel cell stack and system models would benefit from fewer assumptions and simplifications; for example, the assumed constant pressure drop in the humidifier and in the cooling channels and fully humidified membrane. A new optimization could be performed that takes into account not only the operating conditions as design variables but also the geometric parameters of the fuel cell. Indeed, a combination of operating parameters with physico-chemical parameters as design variables would result in a comprehensive optimization of a fuel cell system. Also, the objective function can be modified to reflect the operating conditions of an actual fuel cell application: the weighting factors, set to 1 for this study, could be matched to the particular power cycle of the application, increasing the accuracy of the model. Subsequent papers will reflect this ongoing attempt to increase the sophistication and accuracy of the stack and system models.

## Acknowledgments

Significant contributions to this work were made by former IESVic members, including Greg Iuzzolino, Matthew Guenther and Michael Pastula. Professor Guoqiang Wang of Jilin University has contributed to the development of the GA and SA global optimization algorithms and programs. Financial support from the Natural Science and Engineering Research Council of Canada (NSERC) is gratefully acknowledged.

## References

[1] K. Haraldsson, K. Wipke, Evaluating PEM fuel cell system models, J. Power Sources 126 (1/2) (2004) 88–97.
[2] J.C. Amphlett, R.M. Baumert, R.F. Mann, B.A. Peppley, P.R. Roberge, T.J. Harris, Performance modeling of the Ballard-Mark-Iv solid polymer electrolyte fuel-cell. 1. Mechanistic model development, J. Electrochem. Soc. 142 (1) (1995) 1–8.
[3] J.C. Amphlett, R.F. Mann, B.A. Peppley, P.R. Roberge, A. Rodrigues, A model predicting transient responses of proton exchange membrane fuel cells, J. Power Sources 61 (1/2) (1996) 183–188.
[4] R.F. Mann, J.C. Amphlett, M.A.I. Hooper, H.M. Jensen, B.A. Peppley, P.R. Roberge, Development and application of a generalised steady-state electrochemical model for a PEM fuel cell, J. Power Sources 86 (1/2) (2000) 173–180.
[5] M.W. Fowler, R.F. Mann, J.C. Amphlett, B.A. Peppley, P.R. Roberge, Incorporation of voltage degradation into a generalised steady state electrochemical model for a PEM fuel cell, J. Power Sources 106 (1/2) (2002) 274–283.
[6] D. Xue, Z. Dong, Optimal fuel cell system design considering functional performance and production costs, J. Power Sources 76 (1) (1998) 69–80.
[7] R. Cownden, M. Nahon, M.A. Rosen, Modelling and analysis of a solid polymer fuel cell system for transportation applications, Int. J. Hydrogen Energy 26 (6) (2001) 615–623.
[8] G. Wang, Z. Dong, Design optimization of a complex mechanical system using adaptive response surface method, Trans. Can. Soc. Mech. Eng. 24 (1B) (2000) 295–306.
[9] Z. Dong, Stack Assembly Primarily for an Electrochemical Fuel Cell. US Patent, GB 2,336,937A, November 3 (1999).
[10] Z. Dong, Fuel Cell Stack Assembly. P. C. T. P. WO, 99/57781, November 11 (1999).
[11] Z. Dong, J. Shen, Solid Cage Fuel Cell Stack. U. P. Office, 6,720,101 (2004).
[12] Palcan Power Systems Inc. Website: http://www.palcan.com/s/Products/asp, accessed on October 23 (2005).
[13] M. Grujicic, K.M. Chittajallu, Design and optimization of polymer electrolyte membrane (PEM) fuel cells, Appl. Surf. Sci. 227 (1–4) (2004) 56–72.
[14] A. Mawardi, F. Yang, R. Pitchumani, Optimization of the operating parameters of a proton exchange membrane fuel cell for maximum power density, J. Fuel Cell Sci. Technol. 2 (2) (2005) 121–135.
[15] G. Wang, Z. Dong, P. Aitchison, Adaptive response surface method—a global optimization method scheme for approximation-based design problems, J. Eng. Optimizat. 33 (6) (2001) 707–734.
[16] J. Larminie, A. Dicks, Fuel Cell Systems Explained, John Wiley & Sons, New York, 2003.
[17] M. Pastula, Radiator Stack PEM Fuel Cell Architecture, System Modeling and Flow Field Design, Master's Thesis, University of Victoria, 1997.
[18] Z. Dong, Fuel Cell System Modeling Notes, IESVic Document, 2004.
[19] T. Springer, S. Zawodzinksi, S. Gottesfeld, Polymer electrolyte fuel-cell model, J. Electrochem. Soc. 138 (8) (1991) 2334–2342.
[20] F.N. Buchi, G.G. Scherer, In-situ resistance measurements of Nafion(R) 117 membranes in polymer electrolyte fuel cells, J. Electroanal. Chem. 404 (1) (1996) 37–43.
[21] Z. Dong, M. Guenther, G. Iuzzolino, Mathematical modeling of PEM fuel cells and its implementation in MATLAB, Research Report, University of Victoria, 2003.
[22] S.E. Wright, Comparison of the theoretical performance potential of fuel cells and heat engines, Renew. Energy 29 (2) (2004) 179–195.
[23] M. Hussein, J. Baschuk, X. Li, I. Dincer, Thermodynamic analysis of a PEM fuel cell power system, Int. J. Therm. Sci. 44 (2005) 904–911.